JOURNAL OF SPACECRAFT AND ROCKETS
Vol. 32, No. 3, May–June 1995

EOIM-III Mass Spectrometry and Polymer Chemistry: STS 46, July–August 1992

Steven L. Koontz,* Lubert J. Leger,† and James T. Visentine‡
NASA Johnson Space Center, Houston, Texas 77058
Donald E. Hunton§
U.S. Air Force Phillips Laboratory, Hanscomb Air Force Base, Massachusetts 01731
Jon B. Cross¶
Los Alamos National Laboratory, Los Alamos, New Mexico 87545
and
Charles L. Hakes**
Lockheed Engineering and Sciences Company, Houston, Texas 77058

The Evaluation of Oxygen Interactions with Materials III space-flight experiment was developed to obtain benchmark atomic-oxygen reactivity data and was conducted during Space Transportation System Mission 46. We present an overview of the flight experiment and the results of the Lyndon B. Johnson Space Center polymer chemistry and mass-spectrometer–carousel experiments. Mass-spectrometric measurements of gaseous products formed by O-atom reaction with ^{13}C-labeled Kapton™ revealed CO, CO_2, H_2O, NO, and NO_2. By operating the mass spectrometer to detect naturally occurring ionospheric species, we characterized the ambient ionosphere at various times during the flight experiment and detected the gaseous reaction products formed when ambient ions interacted with the ^{13}C Kapton carousel sector. Direct comparison of the results of on-orbit O-atom exposures with those conducted in ground-based laboratory systems, which provide known O-atom fluences and translational energies, demonstrated the strong translational-energy dependence of O-atom reactions with a variety of polymers. A line-of-centers reactive scattering model was shown to provide a reasonably accurate description of the translational-energy dependence of polymer reactions with O atoms at high atom kinetic energies, and a Beckerle–Ceyer model provided an accurate description of O-atom reactivity over a three-order-of-magnitude range in translational energy and a four-order-of-magnitude range in reaction efficiency. Postflight studies of the polymer samples by x-ray photoelectron spectroscopy and infrared spectroscopy demonstrate that O-atom attack is confined to the near-surface region of the sample, that is, within 50 to 100 Å of the surface.

Nomenclature

E_a = apparent activation energy
E_b = energetic barrier to reaction
E_t = kinetic energy of atom-surface collision
R_e = reaction efficiency
T_s = polymer surface temperature
Δ = total residual error in a least-squares regression fit

Introduction

OXYGEN atoms are the most abundant neutral constituents of the Earth's ionosphere[1–4] at altitudes ranging from 200 to 700 km and have been shown to be one of the more important environmental factors involved in the degradation of several important classes of spacecraft materials.[5,6] The primary objective of the Evaluation of Oxygen Interactions with Materials III (EOIM-III) flight experiment was to produce benchmark atomic-oxygen reactivity data for a wide range of materials.[7] Secondary objectives included mass-spectrometric characterization of the gaseous reaction and scattering products formed when the ambient atmosphere interacts with various materials, characterization of the induced environment produced by interaction of the ambient atmosphere with the EOIM-III experiment and the Space Shuttle cargo bay, and characterization of the chemical dynamics of the reaction between O atoms and polymers. In this paper, we present the polymer chemistry and mass-spectrometer results produced by the Johnson Space Center (JSC) component of EOIM-III. EOIM-III was conducted on STS-46 during early August 1992. EOIM-III was a team effort with coinvestigators from all major NASA field centers; the United States Air Force; the European, Japanese, and Canadian space agencies; and the Ballistic Missile Defense Office.

Our approach to achieving EOIM-III objectives was based on comparing measurements of materials samples after exposure to known O-atom fluences in three well-characterized environments: low Earth orbit (LEO), the high-velocity neutral-atom beam (HVAB) system at the Los Alamos National Laboratory (LANL), and a flowing discharge (downstream plasma) system at JSC. Detailed characterization of the exposure environments was accomplished by determining such factors as the O-atom flux and fluence, the O-atom kinetic energy distribution, the sample temperature, the ultraviolet-vacuum ultraviolet (uv-vuv) radiation dose, and sample surface contamination.

The methods and results of the EOIM-III environment characterization effort, including the results of mass-spectrometric measurements of O-atom fluence, are described in detail in the accompanying paper,[1] as are the EOIM-III flight hardware and flight procedures. Preflight and postflight calibration of the EOIM-III mass spectrometer is presented in a second accompanying paper.[2]

Experiment Descriptions and Performance

EOIM-III Space-Flight Experiment Hardware: Mass-Spectrometer–Carousel and Polymer Sample Holders

The mass spectrometer was operated in two different orientations to sample either ambient atmosphere or the induced environment produced by interaction of the ambient with carousel sector surfaces.

Received March 22, 1994; revision received Oct. 20, 1994; accepted for publication Oct. 25, 1994.

*Materials Engineer.
†Branch Chief, Materials. Associate Fellow AIAA.
‡Senior Material Science Technologist. Associate Fellow AIAA.
§Scientist, Ionospheric Physics Branch. Member AIAA.
¶Senior Scientist, Chemical Physics Division, CS2, J-565. Member AIAA.
**Principal Scientist, 2400 NASA Road 1. Member AIAA.

In Fig. 1a, the mass spectrometer is pointed along the cargo-bay normal (−Z in orbiter coordinates); Fig. 1b shows the carousel-sector viewing orientation. The mass spectrometer ion source was of the semiopen variety (as defined by Hayden et al.[8]) and was capable of receiving neutral gas from a 180-deg field of view. With the mass spectrometer in the −Z orientation, only the vertical stabilizer, several cargo-bay components (including the aft bulkhead), and the pods of the orbital maneuvering system are within the field of view of the mass-spectrometer ion source. These surfaces occupy only a small fraction of the field of view of the ion source and, by implication, the rest of the payload.[1,2] A cross-sectional drawing of the mass spectrometer is shown in Fig. 2. The mass spectrometer was operated in both the conventional electron impact mode to detect neutral gases and the ion mode to detect naturally occurring ions. The as-flown altitude and attitude timelines for STS-46 are described in Ref. 1.

In general, the EOIM-III flight hardware performed well during the mission. Before EOIM-III was initiated, the mass spectrometer was operated only as needed to obtain natural and induced environment data for selected vehicle attitudes and operations. Throughout the pre-EOIM-III portion of the mission, the mass spectrometer was pointed in the −Z direction[1,2] and was operated to collect either mass spectra of neutral gases (the electron impact ionization filaments and a repeller grid to exclude ambient ions were both on) in neutral mode, or ambient ions (filaments and repeller grid off) in ion mode, during alternating 1-min intervals. In addition, payload temperature data were recorded throughout the mission using thermocouples placed as described in the accompanying paper.[1]

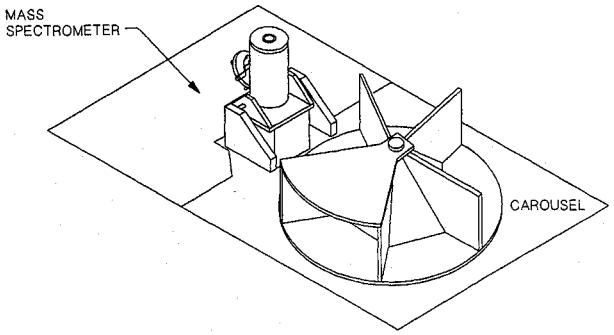

Fig. 1a Mass-spectrometer–carousel configuration for ambient atmosphere measurements.

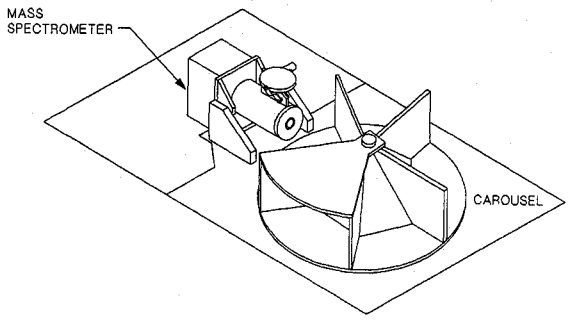

Fig. 1b Mass-spectrometer–carousel configuration for induced environment measurements.

After initiation of the EOIM-III experiment, the EOIM-III payload executed a series of timed operating cycles in which mass-spectrometric measurements of the ambient atmosphere and ionospheric constituents alternated with mass-spectrometric measurements of reaction and scattering products formed when ambient species interacted with various carousel sectors. Each sector was coated with one of the following materials: ^{13}C-labeled Kapton® polyimide prepared by the Jet Propulsion Laboratory, sulfuric-acid-anodized aluminum, Chemglaze Z-306 black polyurethane-based space paint, FEP Teflon®, or Parylene-C coated stainless steel. The carousel sectors were designed so that the geometric field of view of the mass-spectrometer ion source contained only carousel sector surfaces when the mass spectrometer was oriented as shown in Fig. 1b. A movable carousel-sector cover blocked direct incidence of atmospheric species during a portion of each carousel-sector observation period so that the induced environment from both direct ram and scattered ram could be measured.

In addition to carousel–mass-spectrometer operations, heated-tray temperatures were established at 60, 120, and 200°C (prior to placing the orbiter in the ram, −Z VV, attitude for EOIM-III); and timed sample-tray cover movements for the variable exposure trays (VETs) and solar ultraviolet (SUV) trays were initiated.[1,2] The VET cover failed to operate correctly, and all sample specimens received the same nominal O-atom fluence. The SUV and heated-tray experiments operated properly. Two electrical-switching problems were encountered, which have not been explained to date. First, the mass spectrometer did not respond to a power-off command, which led to 13.6 h of unplanned operation early in the mission. Second, the preprogrammed mass-spectrometer–carousel cycle did not initiate properly on the first try, which delayed carousel observations about 6 h. Despite the switching problem, neutral-mode mass spectra were obtained for all carousel segments, and ion-mode spectra were obtained for the Z-306 and the ^{13}C-labeled sectors.

Polymer Chemistry: Materials and Methods

The reactivities of EOIM-III polymer samples were determined by two complementary methods: weight loss and profilometry. In most cases, two disk samples of each polymer were placed in each

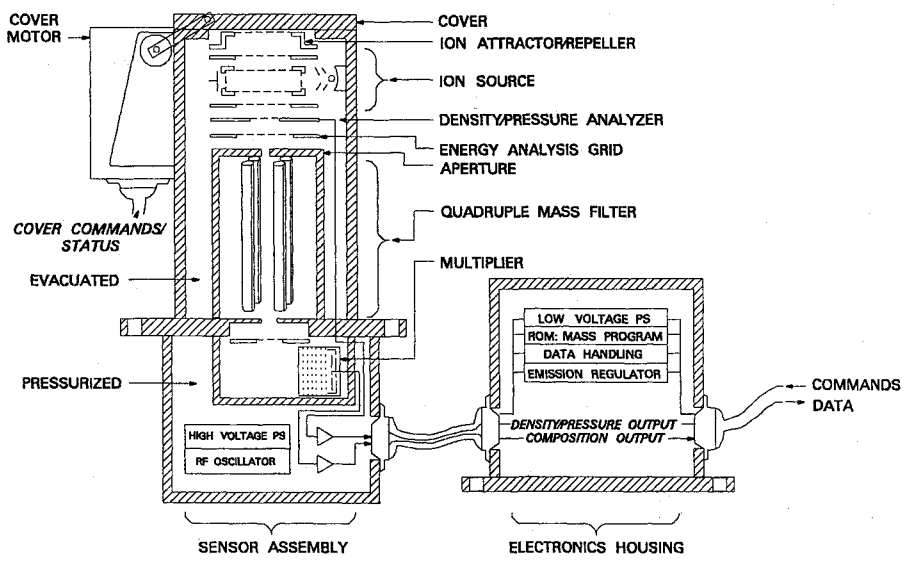

Fig. 2 Cross-sectional drawing of the EOIM-III mass spectrometer.

sample-holder opening. The top sample was directly exposed to the space environment and interacted with atomic oxygen, uv-vuv radiation, and other space environment factors while the underlying sample was exposed only to thermal vacuum. Prior to installation in the EOIM-III sample holders and after postflight removal, both samples were subjected to high-vacuum baking for 48 h at the maximum sample temperature expected on orbit and stored in a desiccator prior to weighing. Before installation in the sample carriers for flight, the samples were cleaned by rinsing briefly with Q Clean® solvent (an ultrahigh-purity cleaning solvent from Thermo Analytical, Inc., Monrovia, California), and air-dried in a laminar-flow hood. Polymer film samples were tested for short-term compatibility with Q Clean before cleaning. Also, the top sample was covered with a high-transparency metal grid, which acted as an etch mask. In this way, the well-known highly directional nature of high-velocity O-atom reactions with polymeric materials was exploited to advantage by producing a regular pattern of ridges on O-atom reactive polymers. The pattern makes profilometry more accurate in the presence of the natural surface irregularities always present on polymer film samples.

All polymer film specimens were used as received from the vendors except for the vacuum baking and cleaning process described. However, the two liquid-crystal polymers, Xydar® and LCP-4100, were also polished because the surface of the as-received material was too rough to permit accurate profilometry even with use of the metal screen etch masks.

Laboratory Support Instrumentation: Apparatus and Methods

Laboratory measurements and calibrations were a key component of the EOIM-III experiment. Effects resulting from sample exposure to laboratory O-atom systems were compared with effects resulting from on-orbit O-atom exposure to gain insight into the reaction mechanism and to verify various approaches to ground-based testing. In addition, the EOIM-III mass spectrometer was calibrated in a ground-based HVAB system. Finally, most materials reactivity determinations were made by postexposure laboratory measurements of polymer specimens for comparison with controls. Weight loss, surface recession by profilometry, scanning-electron-microscope images, X-ray photoelectron spectroscopy (XPS), thermomechanical analysis, and transmission infrared spectroscopy were the most important sample characterization techniques used for the JSC samples. To provide comparison data, two laboratory O-atom systems were used: the flowing discharge and the HVAB. In general, polymer specimens were prepared as for flight on EOIM-III (see above section). Polymers exposed to the HVAB beam were, however, bonded to aluminum heat sinks using a silicone-free epoxy cement to ensure known sample surface temperatures despite heating by beam-source thermal radiation.

The methods and apparatus used to determine the O-atom reactivities of polymers in the flowing discharge (remote plasma) apparatus have been described.[9,10] Briefly, a working gas (10% O_2, 90% Ar) at total pressures on the order of 2 Torr was passed through a 2.45-GHz Evenson discharge cell and flowed downstream from the discharge before coming into contact with the polymer samples. The gas had cooled to room temperature but still contained oxygen atoms in the O^3P electronic ground state. The O-atom concentration was determined by chemiluminescent titration[11,12] using NO_2, and the atom flux on sample surfaces was determined using well-known methods for modeling flowing reaction-diffusion systems.[13] Both the samples and the reactive gas could be heated to determine the Arrhenius activation energies. Unlike the atom-beam and space-flight experiment, both of which deliver O atoms to the polymer surface in the form of a directed beam, the flowing discharge delivers them by diffusion from an isotropic gas in thermal equilibrium with the polymer sample. This does not necessarily imply that the comparison of flowing discharge and directed-beam O-atom processes is invalid in an "apples and oranges" sense, because the O-atom reaction with the sample surface still depends on an O-atom–surface collision. In addition, the flux of molecular oxygen was much higher in the flowing discharge than in the LEO or HVAB environments described above, though large variations in O_2 partial pressure had no observable effects on the reactivity of Kapton, Mylar®, or polyethylene in the flowing discharge system.[9,10,13] Polymer reactivity in this system was determined by periodically venting the system and weighing the polymer specimens on a six-place laboratory balance. The observed mass loss was always significantly greater than any water adsorption or desorption effects.

The HVAB has been described.[14,15] Briefly, a laser-sustained gaseous discharge (50% O_2-Ar or O_2-Ne at pressures on the order of 2000 Torr) undergoes supersonic nozzle expansion to form a seeded beam of oxygen atoms (predominantly in the O^3P electronic ground state as a result of collisional processes during expansion) and inert-gas atoms. The average kinetic energy can be varied between 0.4 and 3 eV. Beam fluxes and velocity distribution functions were determined directly using well-known time-of-flight (TOF) methods.[14–16] The O-atom beam used for calibration and characterization of the EOIM-III flight mass spectrometer was also used to support polymer reaction efficiency measurements.

The typical polymer film temperature during exposure to the O-atom beam was 45°C, and the samples could be heated to determine Arrhenius activation energies. Gaseous reaction products were detected using phase-sensitive (modulated beam) mass-spectrometric detection techniques[15] to reject vacuum-system background.

Results and Discussion: Mass-Spectrometer–Carousel System

The mass-spectrometer–carousel system produced about 48,000 neutral and ion mass spectra during STS-46. Typical ram mass spectra taken during the European Retrievable Carrier (EURECA) postdeployment ram orientation period (altitude 430 km) and at the beginning of the EOIM-III (altitude 230 km) are shown in Figs. 3a and 3b, respectively. For comparison purposes, a typical mass spectrum produced during the calibration process at LANL is shown in Fig. 4, where the O-atom flux was 3.9×10^{15} atoms/cm^2 · s, the argon atom flux was 4.1×10^{15} atoms/cm^2 · s, and the O-atom kinetic energy was 2 eV. Atomic oxygen is visible at mass 16 in Figs. 3 and 4, with water at mass 18 and with the OH^+ ion at mass 17. Molecular oxygen is visible at mass 32 in both figures and is formed by recombination of atomic oxygen in the mass-spectrometer ion source (neither the HVAB beam or the LEO environment contains significant amounts of O_2). The mass-40 and -20 peaks in Fig. 4 are from Ar^+ and Ar^{++}, respectively.

Figure 3 shows a number of features not apparent in Fig. 4. The intense peak at mass 28 amu is produced by molecular nitrogen, a natural component of the atmosphere at Space Shuttle operating altitudes; the associated atomic-nitrogen fragment is visible at mass 14. The mass peak at 44, with an associated doubly charged peak at 22 as well as an atomic carbon fragment peak at mass 12, is attributed to CO_2. The CO peak (mass 28) is obscured by the N_2 peak at mass 28. The molecules H_2O and CO_2 are not components of the natural environment at Space Shuttle operating altitudes, but can be produced by both active (O-atom reactions with cargo-bay materials) and passive outgassing of Space Shuttle cargo-bay components and the mass spectrometer itself. The low-intensity mass peaks at 23 and 39 amu, which correspond to sodium and potassium (also not components of the natural environment), have been reported in mass spectra produced by satellite-borne instruments,[17] and have been attributed to trace contamination of the ion source.

The high-background current visible in the calibration spectrum (Fig. 4) is the result of scattered uv-vuv radiation from the HVAB source, which was coaxial with the ion flight path and the mass spectrometer. The same high-background current would be visible in the EOIM-III mass spectra if the instrument had been directly facing the sun, but the combination of orbital inclination, β angle, and vehicle attitude precluded that event during STS-46. (The 180-deg field of view applies to the ion source only, not the complete path from ion source to secondary-electron multiplier.) During EOIM-III and the various HVAB calibration experiments, the mass-spectrometric sensitivity decreased as a function of O-atom fluence. However, the O-atom fluence dependence of the mass spectrometer was different in the on-orbit and HVAB environments.[1,2]

Only a 30% loss of signal was noted in the photocurrent background at LANL, while a factor-of-6 decrease in ion current was observed (under constant O-atom flux conditions). The effect of O-

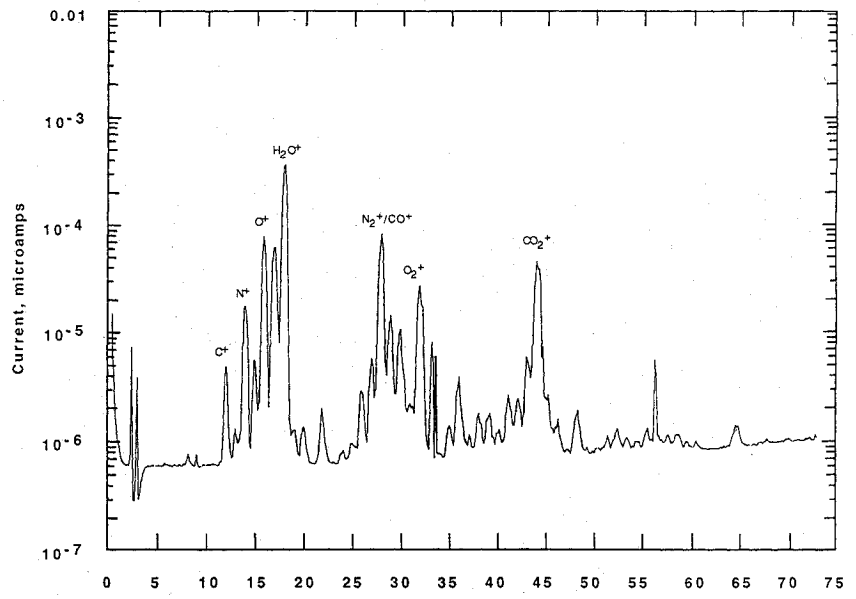

a) Altitude = 231 n.mi.

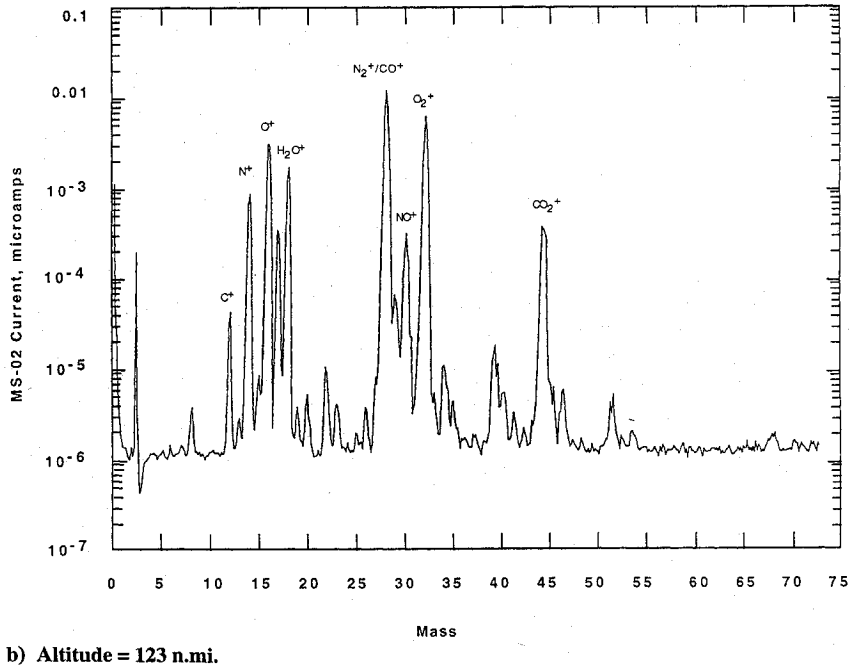

b) Altitude = 123 n.mi.

Fig. 3 Typical mass spectra produced with both the mass-spectrometer axis and the Shuttle $-Z$ axis aligned with the velocity vector (that is, ram-oriented).

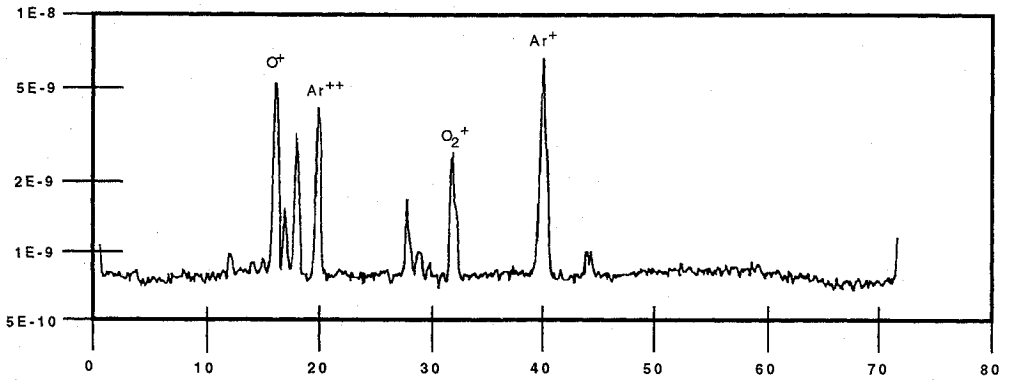

Fig. 4 Typical calibration mass spectra produced by the EOIM-III mass spectrometer in the HVAB at LANL.

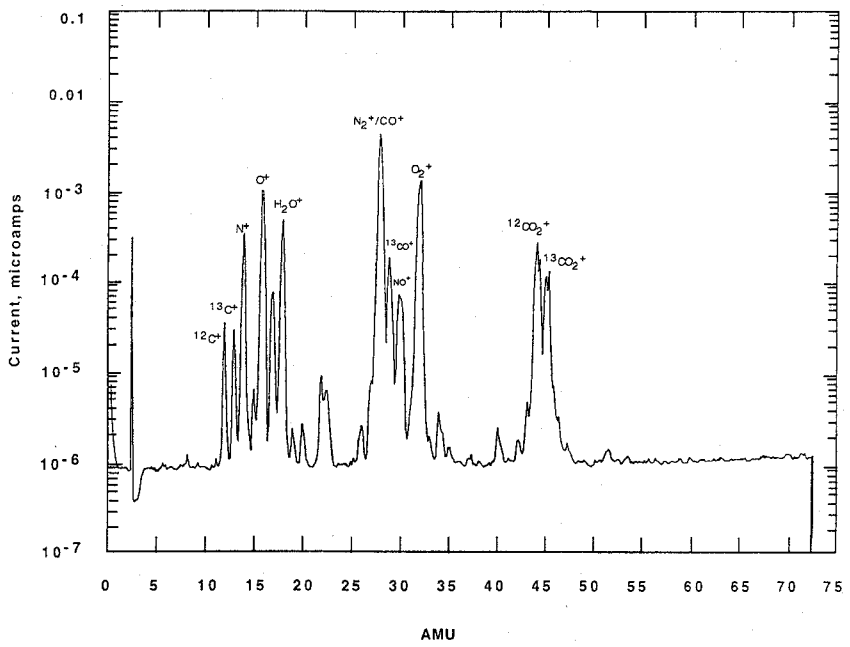

Fig. 5 Mass spectrum of the induced neutral gaseous environment (sector open).

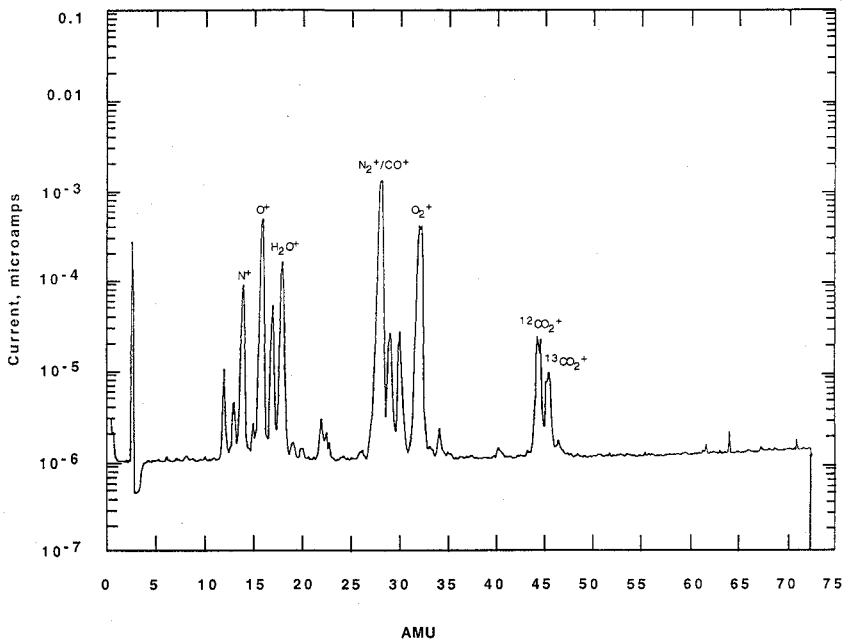

Fig. 6 Mass spectrum of the induced gaseous environment (sector covered).

atom fluence on mass-spectrometer sensitivity is believed to be due to the formation of gold oxide on the surfaces of the gold-plated ion-source optics in the EOIM-III mass spectrometer. This effect was previously reported to occur during mass-spectrometric sampling of ions from flowing discharges with gold sampling orifices.[18] Formation of a dielectric layer on the ion optical elements degrades the sampling efficiency of the ion source. Some degradation of secondary-electron multiplier performance was observed via changes in the amplitude of the photocurrent background during high-fluence calibration experiments at LANL; the effect is small compared to the observed mass-spectrometric sensitivity loss. The formation of gold oxide (Au_2O_3) from gold and molecular oxygen is not observed, because the process is endothermic at 19.3 kcal/mole. In contrast, the formation of gold oxide from gold and atomic oxygen is exothermic at −159 kcal/mole.

Finally, it is interesting to note that different O_2/O ratios were obtained on orbit ($O_2/O = 2.8$) and in the HVAB ($O_2/O = 1.5$). Since O_2 constituted less than 3% of the high-velocity gas entering the mass spectrometer in both environments, the very different O_2/O ratios observed suggest that O-atom recombination and transport processes were different in the two environments.

The immediate conclusion obtained from the comparison of mass-spectrometric performance on orbit and in the laboratory is that simple direct application of the LANL calibration results to the on-orbit data will not give the best accuracy. O-atom fluence estimates based on mass-spectrometric data range from 2.2×10^{20} to 4.7×10^{20} atoms/cm^2, depending on the approach we used to apply the ground-based calibration results to the on-orbit data. Using an empirical sensitivity function derived from the on-orbit signal decay and the zero-fluence ground-based calibration factor, the mass-spectrometric fluence estimate is $(2.3 \pm 0.7) \times 10^{20}$ O atoms/cm^2 as described in Ref. 1. The reported uncertainty is from the ground-based calibration repeatability.

Typical mass spectra of the induced neutral environment in the ^{13}C-labeled Kapton carousel sector are shown in Figs. 5 (sector open to direct ram flux) and 6 (sector cover on, blocking direct ram flux). Comparison with the typical ram mass spectra (Fig. 3) shows that scattered ambient species dominate the induced environment.

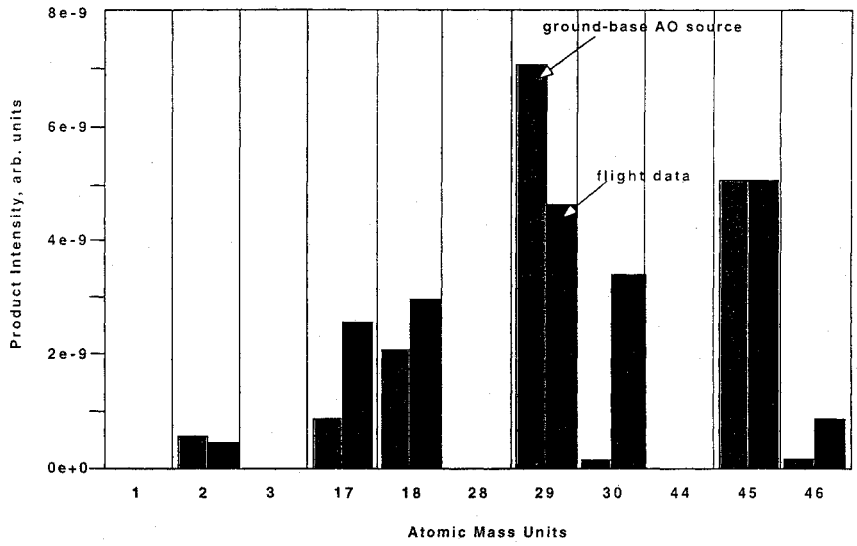

Fig. 7 Gaseous reaction products formed by O-atom reaction in the HVAB compared with EOIM-III measurements.

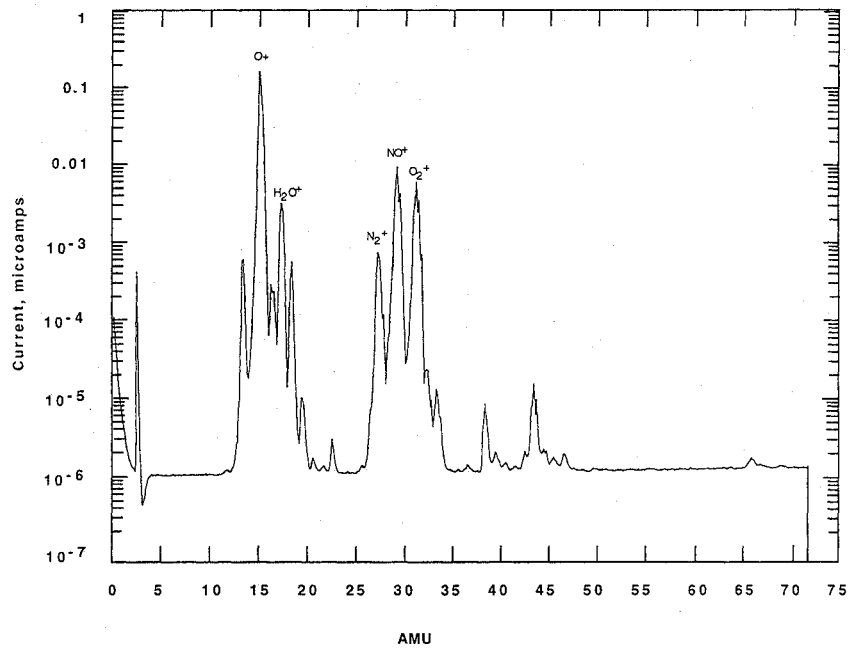

Fig. 8 Mass spectrum of the natural ionospheric plasma environment at 123 n.mi.

Gaseous reaction products are a significant part of the spectra, however, as $^{13}CO_2$ and ^{13}CO are visible in Figs. 5 and 6. Gaseous reaction products formed during exposure of an identical ^{13}C Kapton sample to the HVAB at LANL are compared with EOIM-III measurements in Fig. 7, demonstrating that the same gaseous reaction products are produced in both environments. The higher level of NO, observed at mass 30 in flight, is probably due to environmental interaction processes not directly related to O-atom reactions with polymers. Mechanisms previously proposed to explain the visible spacecraft glow phenomena may explain the high NO signal observed.[19]

Moving the cover over the carousel sector produced little effect except for a net reduction in spectral intensity (Figs. 5 and 6). The fact that the sector cover had little effect is attributed to the scattering of ambient ram species from the EOIM-III pallet near the opening to the carousel sector, as well as scattering of cargo-bay-induced environment gases from aft bulkhead surfaces. With the cover in position over the carousel sector, incomplete momentum accommodation (on surface collision) can result in relatively high-kinetic-energy (high-reactivity) O atoms colliding with the carousel sample surfaces after only two reflections, one from the EOIM-III pallet and one from the sector cover surface that faces the sample compartment.

The EOIM-III mass spectrometer measured ions in the natural and induced environment when the electron impact ionizer and the repeller grid were turned off as described earlier. A typical ambient ion mass spectrum taken with the mass-spectrometer ion source in a ram orientation during EOIM-III operations at a 230-km altitude is shown in Fig. 8. Mass spectra of the induced ionic environment formed by interaction of naturally occurring ionospheric ions with the ^{13}C Kapton carousel sector are shown in Figs. 9 (sector cover off) and 10 (sector cover on). The difference between the ambient ram mass spectra and the induced environments spectra is more notable in this case than in the neutral case of Figs. 5 and 6. Isotope-labeled reaction products are visible in the mass spectra of the Kapton carousel sector and may result from either direct reaction of O^+ ions with the carousel sector surfaces or gas-phase charge exchange of O^+ ions with the gaseous reaction products produced by neutral O-atom attack on the polymer. In contrast with the induced neutral-environment mass spectra of the same carousel sector, mass spectra of the induced ionic or plasma environments dramatically decreased in intensity when the carousel sector cover moved into position, showing that ionospheric plasma ions are efficiently neutralized during collisions with payload surfaces.

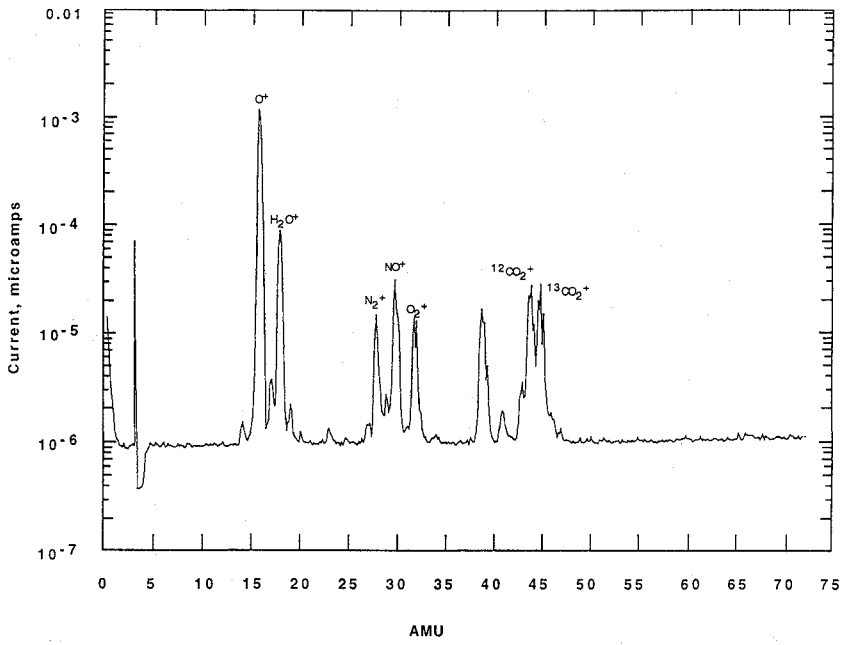

Fig. 9 Mass spectrum of the induced plasma environment in the ^{13}C-labeled Kapton carousel sector (sector open).

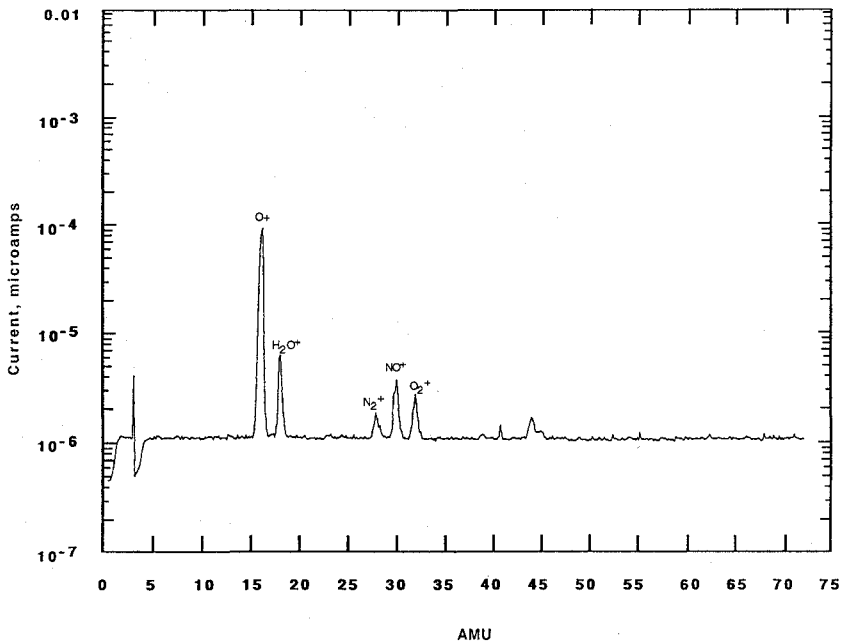

Fig. 10 Mass spectrum of the induced plasma environment in the ^{13}C-labeled Kapton carousel sector (sector covered).

Results and Discussion: O-Atom Reactions with Polymeric Materials

Polymer reaction efficiencies (volume of material removed per incident O atom) determined following exposure on orbit in the EOIM-III passive trays are shown in Table 1, where EOIM-III measurements are compared with those made following previous flight experiments. A comparison of EOIM-III data with data from previous missions demonstrates that the polymer reaction efficiency database has been both enlarged and verified.

The results of replicate measurements of the reaction efficiency of Kapton polyimide demonstrate excellent agreement between the profilometry and weight-loss measurements. Weight loss on four Kapton samples produced a reaction efficiency of $(3.05 \pm 0.1) \times 10^{-24}$ cm^3/atom, whereas profilometry of four different Kapton samples produced a reaction efficiency of $(3.16 \pm 0.1) \times 10^{-24}$ cm^3/atom, using 2.3×10^{20} atoms/cm^2 as the fluence estimate. Both numbers are in excellent agreement with the Kapton reaction efficiencies produced by other on-orbit materials experiments such as STS-8[20] (3×10^{-24}), the Long-Duration Exposure Facility (LDEF)[21] (3.0×10^{-24}), and the Intelsat Solar Array Coupon (ISAC) experiment flown on STS-41[6] (3.1×10^{-24}). The HVAB at LANL was used to produce an independent estimate (independent of MSIS-86 calculations) of the Kapton reaction efficiency as described below. The value of the Kapton reaction efficiency determined in the HVAB is 3.3×10^{-24}, within 10% of the values produced by the flight experiments.

Several general trends in the relationship between O-atom reactivity and molecular structure are visible in Table 1. For example, PE, Tedlar, Tefzel, Kynar, and Teflon are all linear carbon chain polymers with increasing fluorine content and decreasing hydrogen content as we move along the series from polyethylene $[(CH_2CH_2)_n]$ or polypropylene to Teflon $[(CF_2CF_2)_n]$ or FEP Teflon. As can be seen in Table 1, increasing fluorine content results in decreasing O-atom reaction efficiency, as we would expect if hydrogen-atom abstraction is a rate-limiting process and fluorine-atom abstraction occurs to a very limited extent, if at all. Additional evidence supporting the involvement of C–H bond breaking in the O-atom reaction with saturated hydrocarbons can be seen in Table 2, where

Table 1 Polymer reaction efficiencies

Polymer	Reaction efficiency, R_e, 10^{-24} cm^3/atom			
	EOIM-III	STS-8	STS-41	L=DEF
Kapton (LeRC R.R.)	3.1	3.0	3.3	3.0
Eymyd-F (Ethyl Corp.)	2.7			
CR-39 Polycarbonate	6.1	6.0		
Peek (ICI)	3.4		4.3	
Xydar (AMOCO)	2.9			
LCP-4100 (DuPont)	3.2			
Mylar A (DuPont)	3.8	3.9		
PE	4.4	3.7		
HDPE (Phillips, EMH6606)	3.7	3.7	3.5	
Polymethylpentene (PMP, MITSUI)	5.3			
Polypropylene	5.5		4.4	
Tedlar (DuPont)	3.5	3.2		
Tefzel (clear, DuPont)	0.9		0.2	
Tefzel (blue, Raychem)	1.1			
Tefzel (white, Raychem)	0.9			
Kynar (Penwalt)	1.2			
KEL-F (PCTFE, 3M)	0.9			
Halar (Allied)	1.9			
ACLAR 33C (Allied)	1.0			
FEP Teflon (LeRC R.R.)	0.05	<0.03	<0.03	0.3
TFE Teflon (DuPont)	0.06	<0.03		0.5
EYPEL-F, (Ethyl Corp.) Poly(bistrifluoropropylphosphazene)	<0.03			

Table 2 Effects of atom-surface collision energy on the reaction efficiency R_e and the parameters of the empirical Arrhenius equation

Polymer	LEO		HVAB		FDS	
	R_e, 10^{-24} cm^3/atom	E_a, eV	R_e, 10^{-24} cm^3/atom	E_a, eV	$R_e 10^{-24}$ cm^3/atom	E_a eV
Kapton	3.1	0.02	3.3	0.01	2	0.3
Mylar	3.8	0.05	—	—	3	0.4
D4PE	3.8	0.0	—	—	20	0.2
PE	3.7	0.0	—	—	40	0.2
Kynar	1.2	0.0	—	—	0.3	0.4
Tefzel	0.9	0.04	—	—	0.3	0.5
LCP-4100	3.2	0.04	—	—	—	—
Xydar	2.9	0.05	—	—	—	—
CR-39	6.1	0.04	—	—	—	—
Eymyd-F	2.7	0.03	—	—	—	—
Peek	3.4	0.03	—	—	—	—

perdeuteropolyethylene (D4PE) and polyethylene (PE) show a substantial kinetic isotope shift at low atom collision energy in the flowing discharge system (FDS) and virtually no kinetic isotope shift at high atom collision energy during EOIM-III.

The EOIM-III reaction efficiency for Teflon is intermediate between that reported from STS-8 (Ref. 20) and LDEF.[22] We attribute the observed range of reaction efficiency values to different net doses of solar uv-vuv radiation in the different mission environments. Vuv photochemistry has been shown to be the controlling factor in the O-atom chemistry of Teflon and Kel-F.[23,22] The EOIM-III payload received a larger vuv radiation dose than STS-8 as a result of the solar inertial hold period following deployment of the EURECA satellite during an earlier portion of the STS-46 mission, and a much lower dose than LDEF. Incorporating two CF_3 groups into a polyimide structure results in a small but detectable change in reaction efficiency, as can be seen by comparing the reaction efficiencies of Kapton polyimide and Eymyd-F. In general, the aromatic polymers displayed significantly lower reaction efficiencies than the linear straight-chain hydrocarbons, with the exception of the polycarbonate. The very low reaction efficiency of the poly(bistrifluoropropylphosphazene)-based polymers X-221, X-222, and Eypel-F, all showing little or no evidence of reaction, confirms earlier work in ground-based test facilities.[24] Eypel-F is a durable, high-temperature elastomer that may find use in spacecraft atomic-oxygen environments.

Table 2 shows the temperature dependence of the polymer reaction efficiencies determined following exposure to known O-atom fluences on the EOIM-III heated trays, in the flowing discharge apparatus, and in the HVAB. The temperature dependence of the O-atom reaction efficiency is shown as an empirical or apparent Arrhenius activation energy E_a, that is, the natural logarithm of the reaction efficiency is plotted against the reciprocal of the polymer sample temperature and E_a is reported as the slope. It should be noted that the atom kinetic energy appears nowhere in this expression, so that the E_a values are really apparent E_a values for a particular O-atom environment. For all the cases examined to date, straight-line Arrhenius plots have been obtained with correlation coefficients between 0.95 and 0.99. Inspection of Table 2 shows that a large decrease in the Arrhenius activation energy is obtained on going from the flowing discharge to the HVAB or orbital environments. The large decrease in activation energy is accompanied by the large increase in reaction efficiency. In the table, $R_e = A \exp[-E_a/kT_s]$ where T_s is the polymer surface temperature and E_a is the apparent activation energy in electron volts.

The O-atom kinetic energy on impact with the polymer surface does not appear in the Arrhenius equation. As a result, the activation energy calculated by this method can vary with O-atom kinetic energy, if atom kinetic energy is available to overcome energetic barriers to reaction as has been previously proposed.[9,10,25] Alternatively, the mechanism of reaction could change as the atom kinetic energy approaches a threshold value. Simple semiempirical power laws or exponential functions have been shown to produce reasonable agreement with the limited data available in the 0.065- to 5.0-eV translational energy range, which suggests that a single reaction

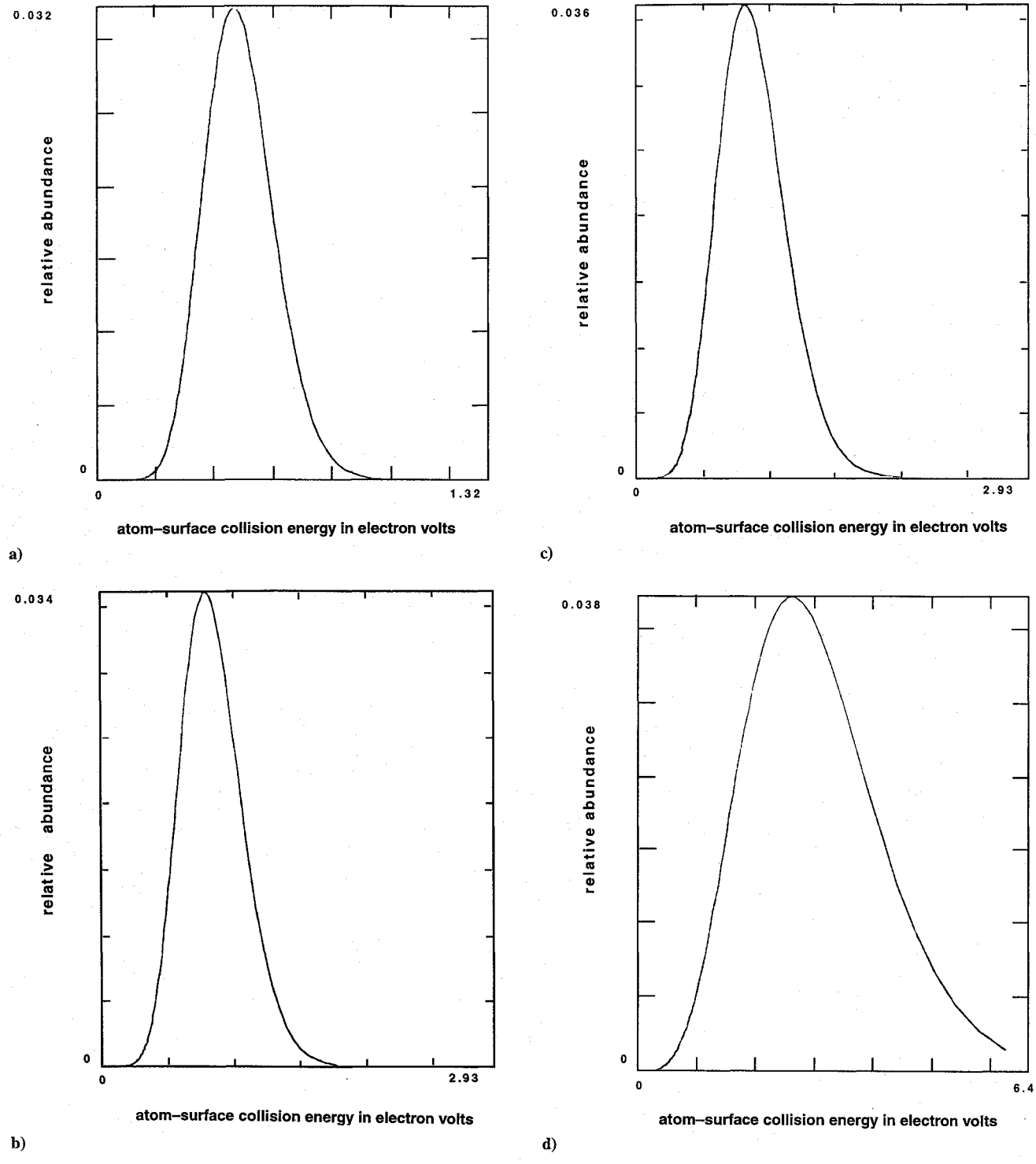

Fig. 11 O-atom kinetic energy distribution functions.

mechanism as well as a single energetic barrier to reaction may determine the reaction efficiency in the O-atom kinetic energy domain of interest. The question cannot be resolved without reaction efficiency data taken at several translational energies between 0.1 and 1.0 eV.

The LANL HVAB was used to obtain reaction efficiency data on Kapton polyimide at average atom kinetic energies of 0.44, 0.72, 0.79, and 2.1 eV. Velocity distribution functions and HVAB composition were measured as described in the subsection "Laboratory Support Instrumentation: Apparatus and Methods." The four O-atom kinetic energy distribution functions are shown in Fig. 11. For comparison purposes, the kinetic energy distribution functions for ram-incident O atoms in LEO (average kinetic energy 5.6 eV) and for O atoms striking a surface immersed in flowing discharge gas (average kinetic energy 0.065 eV) are shown in Fig. 12.

The component of the kinetic energy normal to the surface plane during collision with the surface and the total O-atom kinetic energy are the same for the O-atom directed beam on orbit and in the HVAB. In the case of the thermalized gas in the flowing discharge, the component of the kinetic energy that is normal to the surface plane during collision with the surface and the total O-atom kinetic energy are not the same. The total kinetic energy distribution on surface collision in the flowing discharge (see Fig. 12) was calculated using well-known molecular-effusion-beam methods. The component of the total kinetic energy normal to the surface plane is often used in surface reactive scattering experiments on surfaces having well-defined surface structures.[26] In the flowing discharge environment, the total kinetic energy on surface collision is probably more appropriate in the case of polymer films, which are expected to be

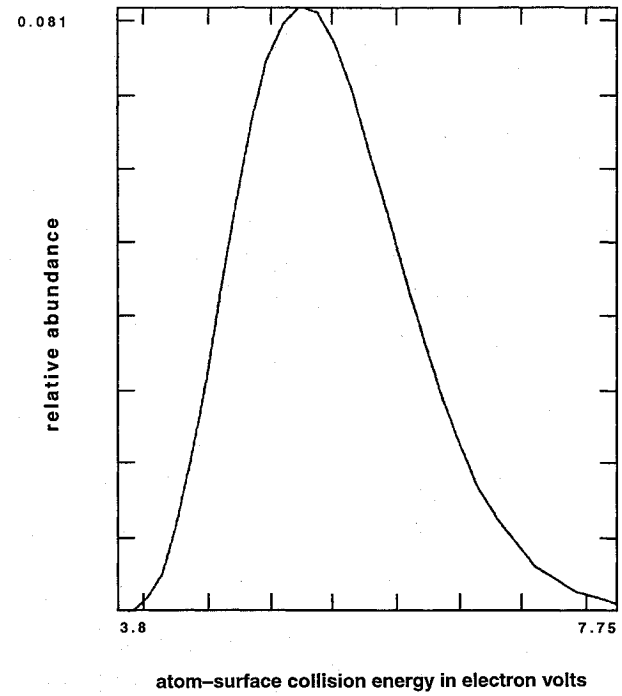

a) LEO environment

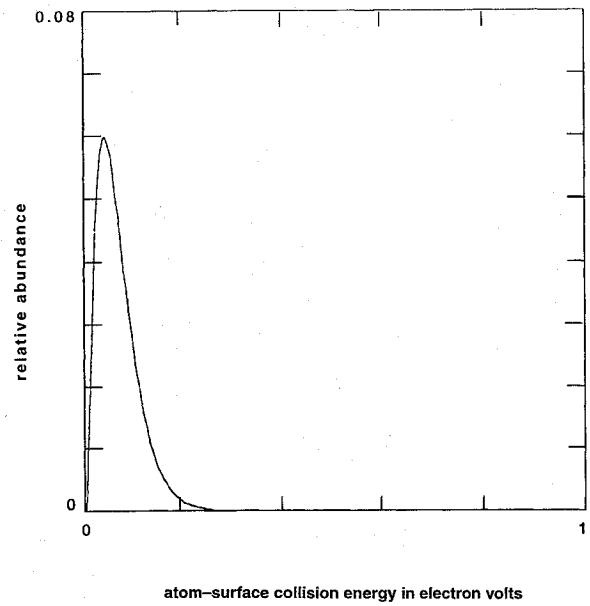

b) Flowing discharge

Fig. 12 O-atom kinetic energy distribution functions.

rough on a molecular scale and show no preferred orientation of chemical bonds.

In Fig. 13, the measured reaction efficiency of Kapton polyimide is plotted against the first moment (average value) of the kinetic energy distributions described in the previous paragraph (Figs. 11 and 12). A rapid increase in reaction efficiency is seen between 0.065 and 1.0 eV, followed by relatively little change between 1.0 and 5.6 eV. The data shown in Fig. 13 suggest that the dynamics of the reaction of O atoms with polymers may be described with a line-of-centers[27] or a Beckerle et al.[26] model of the kinetic energy dependence of the reaction probability. Such models have proven successful in describing the translational energy dependence of a number of gas-phase and surface reactive scattering processes.[26–28] A simple direct fit of the data plotted in Fig. 13 to such a model is an oversimplification, given the width of the velocity distribution functions. A more accurate test of the translational energy dependence hypothesis is needed.

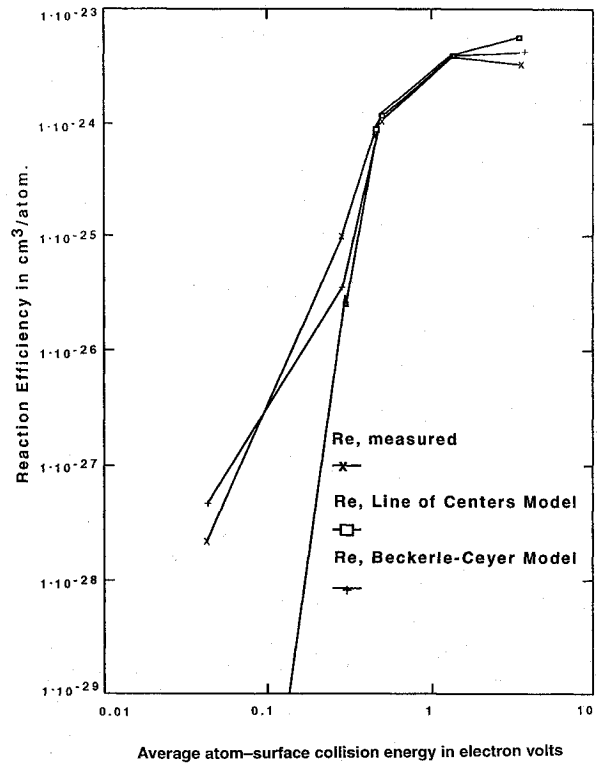

Fig. 13 Measured and predicted R_e values for Kapton polyimide plotted against the average value of the O-atom kinetic energy on collision with the polymer surface for the environments of Figs. 14 and 15.

To test the hypothesis that the simple reactive scattering models provide a reasonable description of the reaction dynamics of O atoms with polymers, we form the convolution integral of the function that describes the kinetic energy dependence of the reaction probability with the normalized kinetic energy distribution function $f(E_t)$ (as shown in the equations below), and then determine if the data on R_e vs $f(E_t)$ can be fitted with the resulting function. Finally, we ask if the R_e equation, with the parameters A, E_b, and n determined by least-squares curve fitting to the HVAB data, can predict values of R_e for the flowing discharge and on-orbit environments.

The model equations are

1) Line-of-centers model:

$$R_e = \int_0^\infty A\left(1 - \frac{E_b}{E_t}\right) f(E_t)\,\mathrm{d}E_t$$

$$1 - \frac{E_b}{E_t} = 0 \quad \text{if} \quad E_t < E_b \tag{1}$$

$$A = 5.10 \times 10^{-24}\,\mathrm{cm}^3/\mathrm{atom}, \qquad E_b = 0.62\,\mathrm{ev}, \qquad \Delta = 0.036$$

2) Beckerle–Ceyer model:

$$R_e = \int_0^\infty \frac{A}{1 + e^{-n(E_t - E_b)}} f(E_t)\,\mathrm{d}E_t \tag{2}$$

$$A = 3.7 \times 10^{-24}, \quad n = 10, \quad E_b = 0.98, \quad \Delta = 0.008$$

Here R_e, as defined by the R_e equations, in (1) and (2), is the average of a large number of reaction efficiencies, one for each kinetic energy interval in the kinetic energy distribution function of interest. The R_e equations allow us to calculate the reaction efficiency given the normalized kinetic energy distribution function $f(E_t)$ and values for the parameters E_b, the magnitude of the energetic barrier to reaction, and A, the limiting reaction efficiency at high kinetic energies. The quantity Δ is the residual sum-of-squares error at the conclusion of the curve-fitting process.

We test the hypothesis represented by an R_e equation as follows. First, because a priori values for A and E_b are not available,

a Gaussian least-squares curve-fitting process is used with A and E_b as adjustable parameters. Thus A, E_b, and any other adjustable parameters are varied until the R_e equation gives the best fit (minimum) Δ to the R_e data produced by exposing Kapton samples in the four different atom-beam kinetic energy distribution functions shown in Fig. 12. The success of the curve-fitting operation, in terms of both the reasonableness of the A and E_a values obtained and the magnitude of the sum-of-squares error at the end of the curve-fitting process, is one test of the validity of the hypothesis. A second test involves asking how accurately an R_e equation, with A and E_b values determined as described above, can predict R_e values for kinetic energy distributions well outside the range of values used in the least squares process. Specifically, can an R_e equation, with A and E_b determined from HVAB data, predict R_e values obtained from the flowing discharge and EOIM-III experiments?

The predictions of the R_e equations are plotted with the measured R_e values in Fig. 13. Clearly, both R_e equations provide a reasonably accurate description of the kinetic energy dependence of the Kapton R_e for the HVAB and on-orbit data. The two models differ significantly in their ability to accurately predict the R_e in the flowing discharge apparatus. The Beckerle–Ceyer model produces reasonably accurate predictions of the Kapton R_e over a three-order-of-magnitude range of O-atom kinetic energy and a four-order-of-magnitude range in R_e. Failure of the line-of-centers model to predict R_e at thermal energies suggests that the potential energy surface describing the reactive collision may change in such a way that E_b varies with collision energy. The Beckerle–Ceyer model, with parameters estimated for Kapton, is a useful tool for making reasonable estimates of R_e for a variety of polymers in both thermal and hyperthermal O-atom environments, as can be seen by comparison of the data in Tables 1 and 2 with Fig. 13. The Beckerle–Ceyer model was developed to explain the translational-energy dependence of the collisionally induced chemisorption of methane physisorbed on Ni. Chemisorption was induced by surface collisions of high-velocity Ar atoms with the physisorbed methane. It is interesting to note that the values of n and E_b obtained in the atomic-oxygen study reported here are comparable to the values obtained by Beckerle and Ceyer ($n = 11$ eV^{-1}, $E_b = 1.4$ eV). The values of A are more difficult to compare, because A is a limiting R_e in the R_e models, but a limiting reaction probability in the Beckerle–Ceyer study. However, a limiting reaction efficiency of 1×10^{-24} corresponds to an O-atom reaction probability of 0.1, comparable to the Beckerle–Ceyer A of 0.09.

The results of XPS studies of several polymers are shown in Table 3 (expressed as atom percent) where samples exposed to the O-atom flux during EOIM-III are compared with flight controls (that is, samples exposed to the space vacuum during EOIM-III but not to O-atom flux). All the polymer samples show measurable increases in surface oxygen content accompanied by surface depletion of carbon. However, the net disturbance of the surface atomic composition is relatively small at 10 to 15 at. %. In contrast, infrared absorption spectra of the polymer sample films show no significant difference between the samples exposed to ram atomic oxygen and the control sample, except a slightly smaller absorbency value for the exposed samples, which were thinner than the controls as a result of O-atom

Table 3 Surface composition of EOIM-III polymer films

	Composition, at.%									
	O-atom reaction surface					Control surface				
Polymer	C	O	N	F	Si	C	O	N	F	Si
Kapton	64.3	23.2	5.7	0.0	6.8	79.7	13.3	5.7	0.0	1.1
Mylar	71.2	24.2	0.6	0.8	2.2	75.1	22.7	0.1	0.3	1.8
Peek	49.3	36.1	2.4	5.2	6.9	81.0	15.9	0.6	0.4	2.2
PE	80.4	14.2	1.5	0.0	3.8	94.8	3.4	0.0	0.0	1.8
PMP	86.9	9.1	0.3	0.5	3.2	97.3	1.8	0.0	0.0	0.9

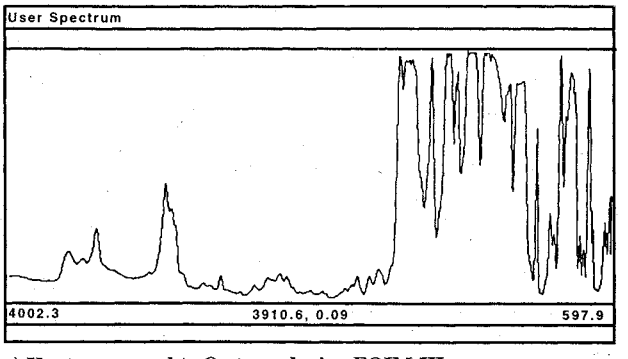

a) Kapton exposed to O atoms during EOIM-III

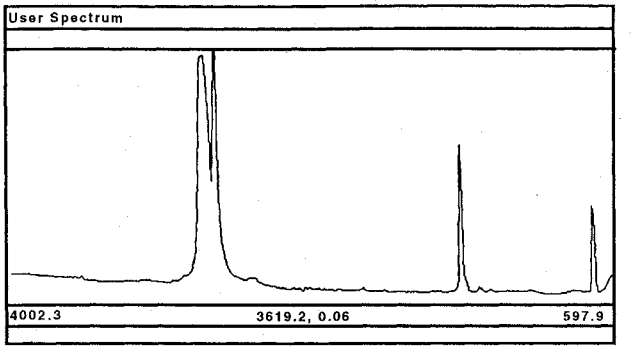

c) PE exposed to O atoms during EOIM-III

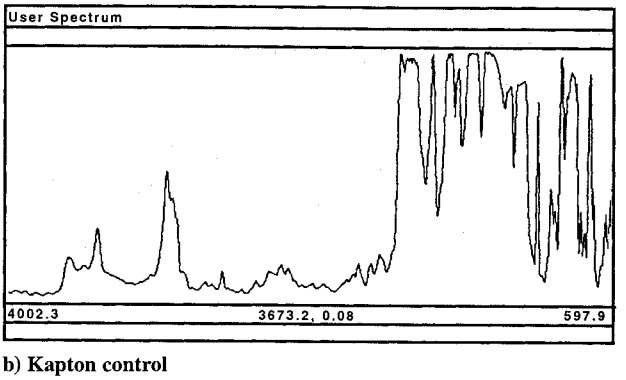

b) Kapton control

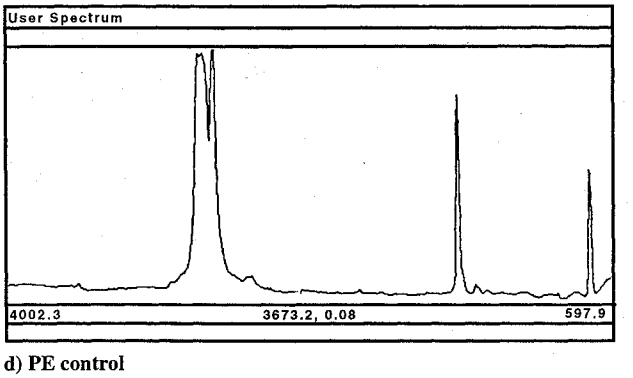

d) PE control

Fig. 14 Typical infrared absorbency spectra of Kapton and PE from EOIM-III.

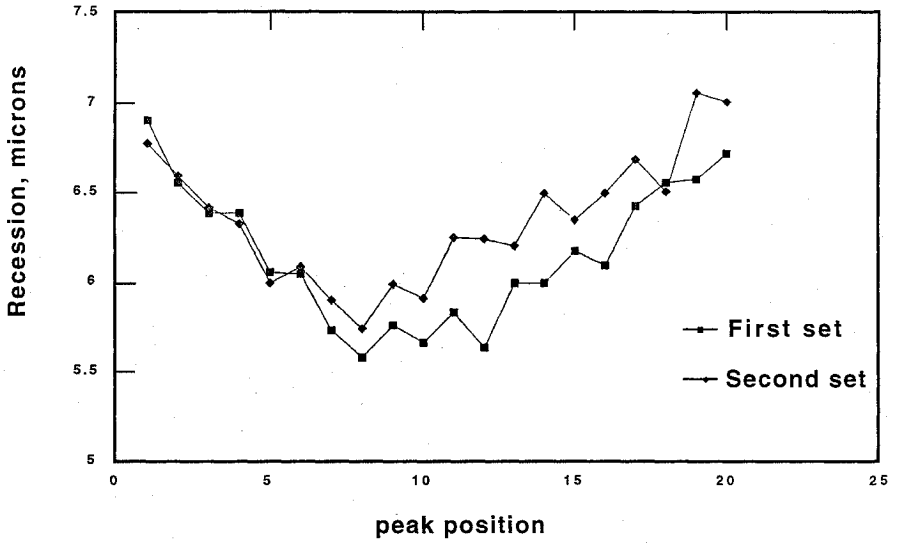

Fig. 15 Profilometry measurements of Kapton film specimens covered with a high-transparency metal grid etch mask.

reaction. Bulk incorporation of O atoms at 1 to 10 at. %. is expected to produce easily detected infrared spectral features.[29] Because the XPS method has a sampling depth on the order of 0 to 50 Å, we can conclude that O-atom reaction processes are confined to the near-surface region of the polymer, with no significant reaction processes occurring at the greater depths sampled by infrared spectroscopy. Typical infrared adsorbance spectra of Kapton and polyethylene that were exposed to the ram O-atom flux during EOIM-III are compared to those of the corresponding flight controls in Fig. 14.

Finally, profilometry and weight-loss measurements on JSC polymer samples revealed some interesting configuration interaction effects produced by the sample holders themselves. Thin metal screens were placed in front of most polymer samples on EOIM-III to act as etch masks and help provide more accurate profilometry. However, the profilometry measurements showed more surface recession near the edge of the 2.065-cm-diam sample holder opening and less recession near the center (Fig. 15). The effect is probably a result of the 45-deg bevel machined into the circular sample openings in the sample holders. High-velocity oxygen atoms can scatter off the beveled surface and onto the sample, effectively increasing the O-atom flux and fluence nearest the edge of the sample-holder opening.

Conclusions

Despite some minor payload timing and switching problems, the EOIM-III flight experiment achieved all of its objectives. A well-characterized, short-term, high-fluence O-atom exposure was provided for a large number of materials, many of which had never before been exposed to the atomic-oxygen environment in LEO. Detailed definition of the sample exposure history is provided in Refs. 1 and 2. The mass-spectrometer–carousel experiment produced over 48,000 mass spectra, providing detailed characterization of both the natural and the induced environment. The mass-spectrometric database will prove a valuable resource in future years for the verification of various models of rarefied-gas and plasma flow around spacecraft. The gaseous reaction products of various polymer species have been determined in the LEO environment, and reactions of ambient O^+ ions have been observed. Finally, by comparing measurements of polymer reaction efficiency produced in different well-characterized environments, we have determined the dependence of the polymer reaction efficiency on O-atom kinetic energy in an unequivocal way. Reaction efficiency data produced in the HVAB system at several different O-atom kinetic energies were shown to be described by the Beckerle[28] reactive scattering model with an energy barrier of 0.98 eV. The same equation made reasonably accurate predictions of reaction efficiencies in the LEO environment and in the laboratory flowing discharge at JSC. The apparent activation energy for surface recession, defined in terms of polymer temperature only, showed a marked decrease in magnitude as the O-atom translational energy increased, a result that is expected if O-atom kinetic energy is directly available to overcome energetic barriers to reaction.

References

[1]Koontz, S. L., Leger, L. J., Rickman, S. L., Hakes, C. L., Bui, D. T., Hunton, D. E., and Cross, J. B., "Oxygen Interactions with Materials III—Mission and Induced Environments," *Journal of Spacecraft and Rockets*, Vol. 32, No. 3, 1995, pp. 475–482.

[2]Cross, J. B., Koontz, S. L., and Hunton, D., "Flight Mass-Spectrometer Calibration in a High-Velocity Atomic-Oxygen Beam," *Journal of Spacecraft and Rockets*, Vol. 32, No. 3, 1995, pp. 496–501.

[3]Jursa, A. S. (ed.), *Handbook of Geophysics and the Space Environment*, Air Force Geophysics Lab., U.S. Air Force (National Technical Information Service), 1985, Chap. 14, pp. 14-38–14-39.

[4]Hedin, A. E., "A Revised Thermospheric Model Based on Mass Spectrometer and Incoherent Scatter Data: MSIS-83," *Journal of Geophyical Research*, Vol. 88, No. 10, 1983, pp. 170–188.

[5]Leger, L. J., Visentine, J. T., and Santos-Mason, B., "Selected Materials Issues Associated with Space Station Freedom," *SAMPE Quarterly*, Vol. 18, No. 2, 1987, pp. 48–54.

[6]Koontz, S., King, G., Dunnet, A., Kirkendahl, T., Linton, R., and Vaughn, J., "The ISAC Atomic Oxygen Flight Experiment," *Journal of Spacecraft and Rockets*, Vol. 31, No. 3, 1994, pp. 475–481.

[7]Visentine, J. T., and Leger, L. J., "Materials Interactions with the Low-Earth Orbit Environment: Accurate Reaction Rate Measurements," AIAA Paper 85-7019, Nov. 1985.

[8]Hayden, L. J., Nier, A. O., French, J. B., Reid, N. M., and Ducket, R. J., "The Characteristics of an Open Source Mass Spectrometer Under Conditions Simulating Upper Atmosphere Flight," *International Journal of Mass Spectroscopy and Ion Physics*, Vol. 15, 1974, pp. 37–47.

[9]Koontz, S. L., Albyn, K., and Leger, L. J., "Atomic Oxygen Testing with Thermal Atom Systems: A Critical Evaluation," *Journal of Spacecraft and Rockets*, Vol. 28, No. 3, 1991, pp. 315–323.

[10]Koontz, S. L., Albyn, K., and Leger, L., "Materials Selection for Long Life in Low Earth Orbit," *Journal of the Institute of Environmental Sciences*, March/April 1990, pp. 50–59.

[11]Clyne, M. A. A., and Nip, W. S., "Generation and Measurement of Atom and Radical Concentrations in Flow Systems," *Reactive Intermediates in the Gas Phase*, edited by D. W. Setzer, Academic, New York, 1979, pp. 1–57.

[12]Huie, R. E., and Herron, J. T., "Reactions of Atomic Oxygen (O^3P) with Organic Compounds," *Progress in Reaction Kinetics*, Vol. 8, No. 1, 1975, pp. 1–80.

[13]Koontz, S. L., and Nordine, P., "The Reaction Efficiency of Thermal Energy Oxygen Atoms with Polymeric Materials," *Materials Degradation in Low Earth Orbit (LEO)*, edited by B. A. Banks and V. Srinivasan, The Minerals, Metals and Materials Soc., Warrendale, PA, 1990, pp. 189–205.

[14]Cross, J. B., and Blais, N. C., *High Energy/Intensity CW Atomic Oxygen Beam Source*, edited by E. P. Mundt, D. P. Weaver, and D. H. Campbell, Vol. 116, Progress in Aeronautics and Astronautics, AIAA, Washington, DC, 1989, pp. 143–155.

[15]Cross, J. B., Koontz, S. L., Gregory, J. C., and Edgell, M. J., "Hyperthermal Atomic Oxygen Reactions with Kapton and Polyethylene," *Materials Degradation in Low Earth Orbit (LEO)*, edited by B. A. Banks and V. Srinivasan, Minerals, Metals and Materials Soc., Warrendale, PA, 1990, pp. 1–13.

[16]Koontz, S. L., Cross, J. B., and Lan, E., "Characterization and Calibration of the EOIM-III Flight Mass Spectrometer in a High Velocity Atom Beam," *Materials Degradation in Low Earth Orbit (LEO)*, edited by V. Srinivasan and B.A. Banks, Materials, Metals and Minerals Soc., Warrendale, PA, 1990, pp. 155–174.

[17]Hanson, W. B., Sanatani, S., and Hoffman, J.H., "Ion Sputtering from Satellite Surfaces," *Journal of Geophysical Research*, Vol. 86, No. A13, 1981, pp. 11,350–11,356.

[18]Fergeson, E. E., Feshenfeld, F. C., and Schmeltenkoph, A. L., "Flowing Afterglow Measurements," *Advances in Atomic and Molecular Physics*, Vol. 5, Academic, New York, 1969, pp. 12, 13.

[19]Swenson, G. R., and Meyerott, R. E., "Spacecraft Ram Cloud Exchange and N_2 LBH Glow," *Geophysical Research Letters*, Vol. 15, No. 2, 1988, pp. 245–248.

[20]Visentine, J. T., Leger, L. J., Kuminecz, J. F., and Spiker, I. K., "STS-8 Atomic Oxygen Effects Experiment," AIAA Paper 85-0415, Jan. 1985.

[21]John, G., Chemistry Dept., Univ. of Alabama, Huntsville, AL, personal communication.

[22]Steigman, A. E., Brinza, D. E., Anderson, M. S., Minton, T. K., Laue, E. G., and Liang, R. H., "An Investigation of the Degradation of Fluorinated Ethylene Propylene (FEP) Copolymer Thermal Blanketing Materials Aboard and in the Laboratory," Jet Propulsion Lab., publication 91-10, California Inst. of Technology, Pasadena, CA, May 1991.

[23]Koontz, S. L., Leger, L. J., Albyn, K. A., and Cross, J., "Ultraviolet Radiation/Atomic Oxygen Synergism in Materials Reactivity," *Journal of Spacecraft and Rockets*, Vol. 27, No. 5, 1990, pp. 346–348.

[24]Fewell, L., and Fenney, L., *Polymer Communications*, Vol. 32, No. 13, 1991, pp. 393–396.

[25]Arnold, G. S., Peplinski, D. R., and Cascarano, F. M., "Translational Energy Dependence of the Reaction of Atomic Oxygen with Polyimide Films," *Journal of Spacecraft and Rockets*, Vol. 24, No. 5, 1987, pp. 454–458.

[26]Stienfeld, J. I., Francisco, J. S., and Hase, W. L., "Dynamics of Bimolecular Collisions," *Chemical Kinetics and Dynamics*, Prentice–Hall, Englewood Cliffs, NJ, 1989, Chap. 8, pp. 246–268.

[27]Beckerle, J. D., Johnson, A. D., Yang, Q. Y., and Ceyer, S. T., "Collision Induced Dissociative Chemisorption of CH_4 on Ni: The Mechanism for Chemistry with a Hammer," *Journal of Chemical Physics*, Vol. 91, No. 9, 1989, pp. 5756, 5777.

[28]Gonzalez, U. A., "Influence of Translational Energy upon Reactive Scattering Cross Section: Neutral-Neutral Collisions," *Advances in Chemical Physics*, Vol. LXVI, edited by I. Prigogine and S. A. Rice, Wiley, New York, 1987, pp. 231–335.

[29]Iring, M., and Tüdös, F., "Thermal Oxidation of Polyethylene and Polypropylene: Effects of Chemical Structure and Reaction Conditions on the Oxidation Process," *Progress in Polymer Science*, Vol. 15, 1990, pp. 217–262.

R. K. Clark
Associate Editor